# Load distribution in a roller-type rotor blade bearing

IOP Conf. Series: Journal of Physics: Conf. Series **1037** (2018) 042016 doi:10.1088/1742-6596/1037/4/042016

# Load distribution in a roller-type rotor blade bearing

**Matthias Stammler[1], Sebastian Baust[1], Andreas Reuter[1], Gerhard Poll[2]**

[1]Fraunhofer IWES, Am Schleusengraben 22, 21029 Hamburg, Germany;

[2]IMKT, Leibniz Universität Hannover, Welfengarten 1 A, 30167 Hanover, Germany

E-Mail: matthias.stammler@iwes.fraunhofer.de

**Abstract**. Pitch bearings of wind turbines are large, grease-lubricated rolling bearings that connect the rotor blades with the rotor hub. Rolling bearings are the standard bearing type for this application. Most blade bearings are four-point bearings with one or two rows. Three-row roller bearings with two axial rows and one radial row have higher costs, but are an increasingly used alternative. Both rotor blade and rotor hub have a varying stiffness along the circumference of the bearing rings. This results in rotationally non-symmetric load sharing (load distributions) of the bearing rollers. The load distribution depends on the pitch angle, the load magnitude and the load angle. In this paper, we evaluate the load sharing of such a three-row bearing for a reference wind turbine of the 3 MW-class, taking account of the stiffness of the interface parts hub and rotor blade. A set of finite-element simulations with varying loads, load angles and pitch angles has been executed to determine the influence of the named parameters on the loads of the individual rollers. Curve fits of these discrete load points allow the determination of roller loads for any given parameter combination. One application of the results is the determination of the overall bearing load which is a key input for fatigue lifetime calculations.

## 1. Introduction

Pitch bearings (also called blade bearings) are subject to unfavorable operating conditions as they have to accommodate high bending moments while standing still or executing oscillating movements at very low speeds. The connecting parts, especially the rotor blade, provide limited stiffness. Usually, four-point contact ball bearings are used for this application, as they are highly resistant to standstill conditions and large bending moments [1, 2].

With growing rotor diameters, the blade root diameters and blade bearing diameters increase as well. It is not efficient to increase the dimensions of the bearing section accordingly both from a technical and an economical perspective. As such, blade bearings with 5 m diameter do not have twice the height of bearings with 2.5 m diameter, nor do they have twice the ring section width. Thus, larger bearings have a lower relative geometrical stiffness of the bearing section. As a result, four-point bearings are prone to ring ovalization due to loads [3], and the negative results of this effect are increased with lower relative geometrical stiffness. For this reason, three-row roller bearings with two axial rows and one radial row, which have a higher stiffness and constant contact angles, become an attractive alternative solution despite their higher costs.

Pitch bearings connect the rotor hub and the rotor blade. Both interface parts do not have a rotationally symmetrical stiffness. The rotor blade is usually made of a combination of fiber-reinforced plastic (FRP) and wood or foam. Spar caps and shear webs take most of the load introduced by the effect of the wind on the aerodynamic profiles, which results in an asymmetrical load distribution (see Figure

1). The spar caps usually consist of several layers of unidirectional laminate, the shear webs are made of a combination of +/- 45° laminate and wood and/or foam. The blade root is made of quasi-isotropic laminate. Figure 1 displays the aforementioned components of the rotor blade and an exemplary load distribution at the blade root. The load is a pure flap-wise bending moment. The colored area indicates the real load distribution, while the grey area is the load distribution that would result from an ideally stiff tube of the same size.

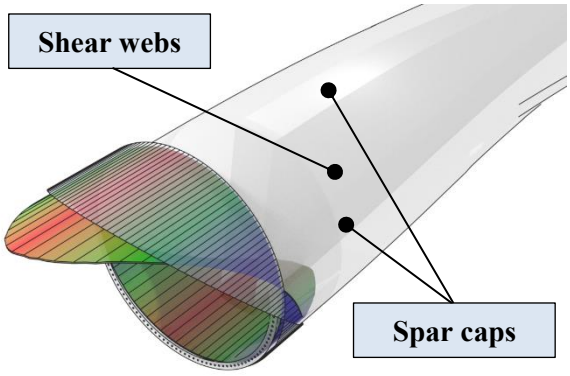


**Figure 1.** Rotor blade: Load transmitting elements and load distribution at the blade root.

It is quite obvious that the load magnitude of the rollers depends on the outer load magnitude. However, due to the varying stiffness along the circumference, both roller load magnitude and relative load distribution of all rollers depend on the outer load angle as well. The outer load angle mostly depends on the current position of the blade, as the blade's weight is contributing to the overall bending moment. The bending moment usually is expressed as a resulting moment $M_{resB}$ of both $M_{yB}$and $M_{xB}$. We used $M_{resB}$ for the simulations as it allows a convenient control of the overall load magnitude. With $M_{resB}$, the information about the axis of the bending moment is not maintained and must be given in another value, which is the outer load angle. A pure $M_{yB}$ has a load angle of 0°, a combination of $M_{yB}$ and $M_{xB}$ of the same magnitude has a load angle of 45°.

Additionally, and for the same reasons as just mentioned, the load sharing does depend on the current pitch angle of the blade. Figure 2 shows the definition of the blade coordinate system and pitch angle used in the present paper. Depending on the controller layout, pitch angles vary from -10 to 90° (the latter results in idling of the turbine).

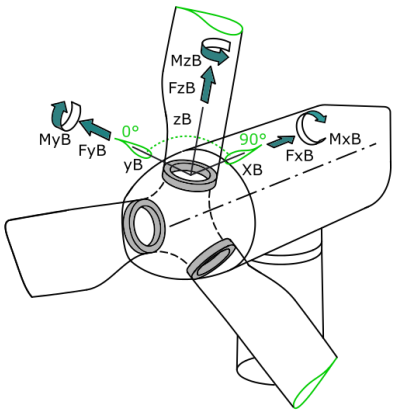


**Figure 2.** Pitch bearing coordinate system (fixed to the hub)

The rotor hub is usually made of cast iron. The asymmetrical stiffness distribution results from the complex geometry of the component [4]. Figure 3 shows a basic rotor hub design and the z-deformation of the blade bearing flange caused by a uniformly distributed force in z-direction ($F_{zB}$).

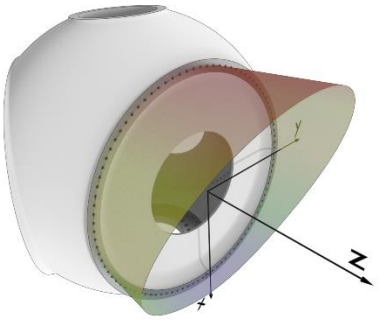


**Figure 3.** Basic rotor hub design of the IWT7.5-164 reference wind turbine [5], displaying the same coordinate system as in Figure 2 and the deformation along the blade baring flange as a reaction to a uniformly distributed force in z-direction

Pitch bearings are bolted to the rotor blade and the rotor hub. To prevent ovalization of the rings, a stiffener plate is commonly used, which is connected to the blade side of the inner ring of the bearing. Due to the high number of rollers in the bearing, global FE-models normally represent the rolling bodies as nonlinear springs connected to the raceways. These simulations do not reproduce the tensions in the raceway correctly, but they do give correct output for the forces, and, in the case of four-point bearings, the contact angles of all rolling elements [3, 6–9]. Sub models with one or few rolling bodies then produce the results for raceway tension and frictional work in the contact [10, 11].

QIU, YAN et al. [12] calculated the influence of negative clearance in a global slewing bearing model. This model contained the balls as solid bodies. They reduced computational time by using a quarter model of a bearing and did not take the interface components into account.

SMOLNICKI and RUSIŃSKI [8] created a global FE-model of a slewing bearing with nonlinear springs representing the rollers and calculated this bearing which is here mounted into a construction crane and reasoned that the interface stiffness distribution cannot be neglected for such calculations.

GAO et al. [9] and AGUIRREBEITIA et al. [6] devised a global FE-model of a slewing bearing with nonlinear springs representing the rollers and used this model to validate theoretical calculations of static capacity.

DAIDIÉ, CHAIB and GHOSN [3] set up a similar FE-model as in [6] and [8] and calculated the load distribution of a model mounted into a crane top. They reasoned in a similar way as SMOLNICKI and RUSIŃSKI that the interface stiffness distribution is of importance for the internal load distribution.

CHEN and WEN evaluated the influence of the rotor hub and a stiffener plate interface on the load distribution within a wind turbine blade bearing [7]. They showed that the hub has significant influence on the load distribution. However, they did not take account of the blade structure but used rotationally symmetric blade root models to apply the loads.

In this paper, we advance the thesis that pitch angle, load angle and load magnitude have an influence on the load distribution of the bearing. The load distribution is the information about the individual load of all rollers in the bearing. We use the results of simulations of a rotor star to derive curve fits of the roller loads. A rotor star consists of a rotor hub, three blade bearings, three stiffener plates and three blades. These results can be used for fatigue lifetime calculations, wear probability estimations and friction torque simulations.

Section 2 of this paper describes the methods of analysis, in particular the FE-model of the bearing and assembly and the settings for the simulation runs. Section 3 presents the results in form of load distribution examples, curve fits for the loads of single elements and a function for $P_{EA}$ depending on load magnitude and angle as well as the pitch angle. Section 4 concludes the paper.

## 2. Methods of analysis

### *2.1. FE-model of the bearing*

In order to easily and automatically analyze and compare the results, a control of nodes and elements and their locations is essential. Consequently, a method connecting predefined nodes subsequently with elements to generate the geometry has been preferred over meshing a solid model in CAD format. Manual creation of each node is time-consuming. Therefore, we created a script to create all elements of the bearing. The readability of ANSYS scripts is limited and implementation of different geometry input data is difficult, thus a MATLAB-routine creates an ANSYS input script for the entire bearing model including bolts and stiffener plate. Within MATLAB, geometrical parameters and roller properties are set. Structurally non-relevant details like sealing grooves were not implemented in the model.

The geometry of a triple-row cylindrical roller bearing is piecewise cyclic-symmetric. However, these bearings do not have equal numbers of roller elements on the axial and radial raceways nor do they have equal numbers of bolt holes in the outer and inner ring. For this reason it is not possible to define one common piece for the bearing. Instead, the cross section of the bearing is divided in four different sectors, see Figure 4: One for the axial (red) and radial (blue) roller raceways, respectively, and one respectively for the inner (green) and outer (yellow) part of the ring containing the bores.

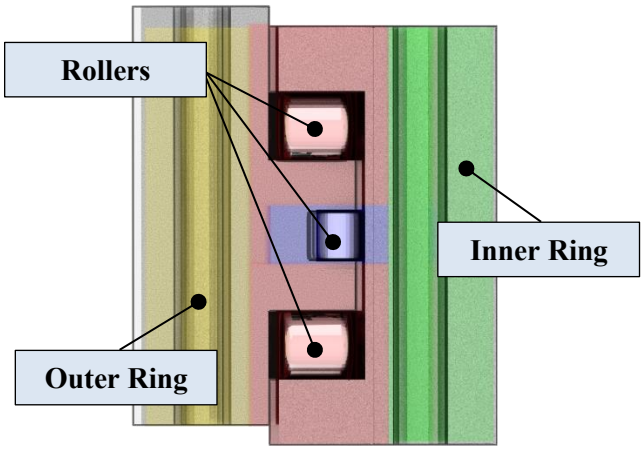


**Figure 4.** Sectors of bearing cross section

The sectors are connected with bonded contacts. The different number of elements on the location of nodes can cause stress singularities at the contact areas. However, these stress singularities at the contact areas do not influence the forces transferred by the rollers as they are located far enough from the roller-raceway contact area.
In order to increase computational efficiency, the roller-raceway contact is not fully modelled with solid rollers and contact elements but substituted by compression-only non-linear springs along the rectangular contact area of roller and raceway. Along the rectangular contact area, rigid beams are placed of which always two beams of the inner and outer raceway respectively connect at one end of the nonlinear spring. Accordingly, one roller element does not consist of one spring but a number of springs N with a stiffness of $K_N = K/N$ respectively. Figure 5 shows such an arrangement with four nonlinear springs (red, COMBIN39 elements) and eight rigid beams (grey, MPC184 elements). The application

of more than one non-linear spring is required due to the modelling technique of the roller-raceway contact. One spring stiffens the roller raceway contact, which leads to unrealistic stress singularities influencing both deformation behavior and roller forces. On the other hand, many springs lead to an unstable system und consequently convergence problems.

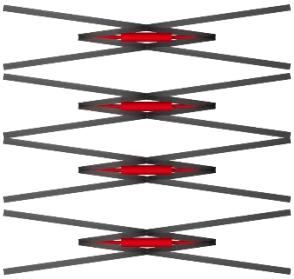

**Figure 5.** COMBIN39 and MPC184 elements representing a roller

To determine the stiffness of the rollers K, single contact simulations were performed and compared against well-known approximation functions for line contacts [13]. The results were transferred into the global bearing model.

Besides the bearing itself, the geometrical parameters and properties of the stiffener plate and hub- as well as blade-bolts for assembly are defined. Again, to increase computational efficiency the bolts are not modelled as solid bodies but as beam elements. They are divided in different sections in order to mirror the characteristics of different bolt segments like shank, traction or thread.

Figure 6 shows the mesh of the FE-model (excluding bolts), where black / red lines indicate the combination of MPC184 and SPRING39 elements

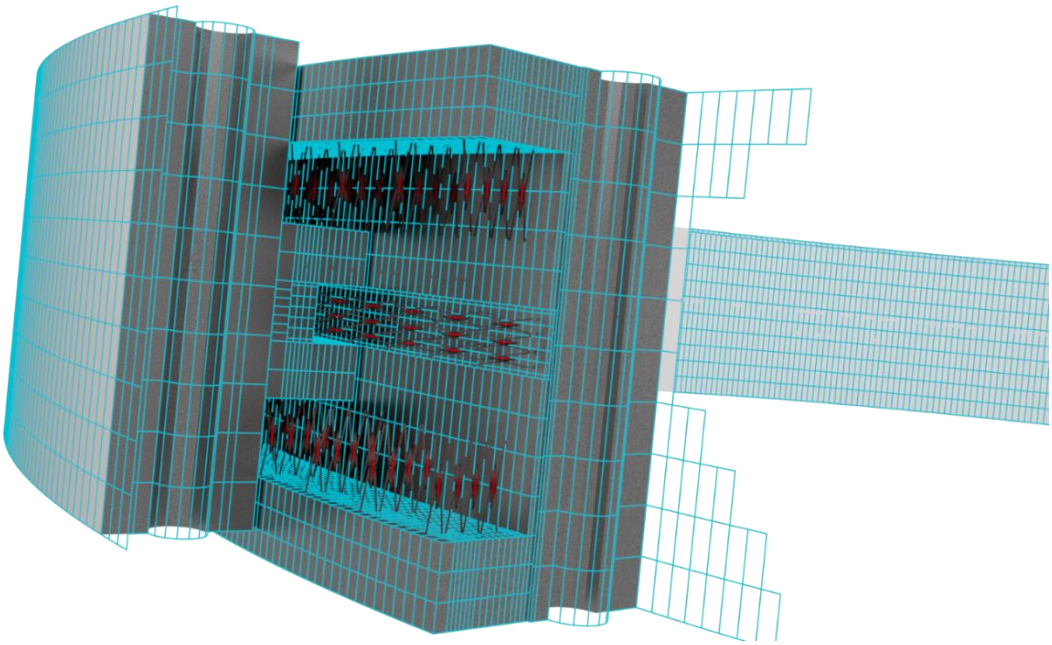

**Figure 6.** Representation of the bearing FE-model: Mesh and rigid beams and nonlinear spring combinations

### *2.2. Rotor star assembly and simulation sets*

The rotor star assembly consists of three bearings, three stiffener plates, three blades and a hub. All parts are generic parts of a 3 MW class turbine. The blades have a length of 54 m and a single spar cap on the pressure and the suction side. The root diameter is 2.3 m. The blade attaches to the outer ring of the bearing.
The following section contains the results of one of the bearings, called primary bearing. This bearing connects to the adjacent parts by a friction contact and pre-tensioned bolts. Although only the results of the primary bearing are used for the later evaluation, the other two bearings and blades must be taken into account to simulate the correct hub stiffness. These bearings are connected by bonded flange contacts without bolts.

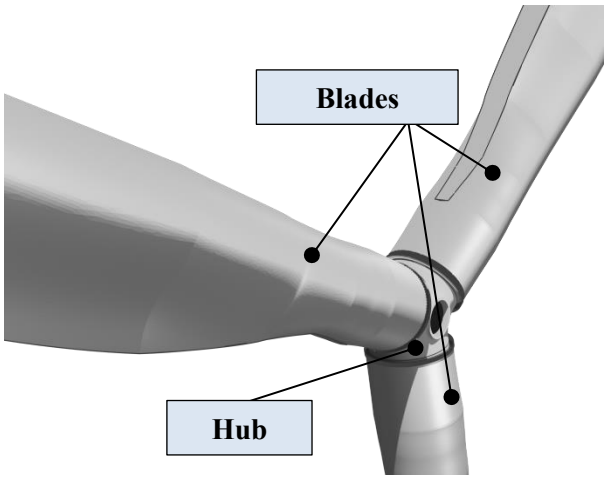


**Figure 7.** Rotor star assembly of a 3MW-class turbine used for simulations

The hub mesh comprises solid elements. The blade mesh is a mixture of solid and shell elements, with solid elements forming the root section. A combination of a relatively stiff spring and stiff beam elements connects the bearings outer ring and the hub. It simulates the interface between bearing and pitch drive and fixes the rotational degree of freedom of the bearings.

To evaluate the thesis of this paper, we did 126 simulation runs with the parameter combinations outlined in Table 1. All parameters represent the operating loads below rated speed of a 3 MW-class turbine with individual pitch control (IPC). The load angle and pitch angle for the secondary and tertiary bearing are constant throughout the simulation set as no significant influence was found. The load magnitude on these bearings is set to one third of the load magnitude of the primary bearing.

**Table 1.** Simulation settings for load magnitude, load angle and pitch angle of the primary bearing

| Parameter | Unit | Steps |
|---|---|---|
| Resulting bending moment $M_{resB}$ | MNm | 6, 8 |
| Load angle | ° | -30 to 30 in steps of 5° |
| Pitch angle | ° | -6 to 24 in steps of 6° |

*Roller load evaluation*

The loads of the individual rollers are the input value for other calculations. In particular it is possible to derive:

- Friction torque
- Rolling contact fatigue lifetime
- Static load capacity

We presented an evaluation of different friction torque models in a former paper [14]. Rolling contact fatigue calculations are part of the ISO 281 [15]. The ISO 281 provides procedures to calculate the summarized roller loads $P_{EA}$ with the outer loads (radial force $F_R$, axial force $F_A$, bending moment $M$) as input, see Equation 1. $d_m$ is the pitch diameter of the bearing. These results apply for an ideally stiff surrounding. Equation 2 then gives the loads of the individual rollers $Q$ for the case of pure bending moment (see Figure 1). $Z$ is the overall number of rolling bodies.

$$P_{EA} = 0.75F_R + F_A + \frac{2M}{d_m} \quad (1)$$

$$Q_j = \frac{2M}{d_m \cdot z} \cdot cos\left(\frac{j}{Z} 2\pi\right), j = [1; Z] \quad (2)$$

In case of rotationally non-symmetric stiffness distributions, Equations 1 and 2 do not apply. A suitable alternative is to calculate the summarized load by the individual roller loads $Q$, see Equation 3, taken from the ISO 281. Note this equation applies for roller bearings, not ball bearings.

$$P_{EA} = \left(\frac{1}{Z}\sum_{j=1}^{Z} Q_j^4\right)^{1/4} Z \quad (3)$$

The simulation results obtained in this work allow to calculate this more exact bearing load, both for the purpose of fatigue life calculations and static capacity evaluations. As mentioned above, fatigue calculations are part of the ISO 281. Static load capacity is part of ISO 76 [16], but is not evaluated within this work.

## 3. Results and discussion

Figure 8 shows a comparison of roller loads of a bearing with stiff interfaces (according to Equation 2) and three different pitch angles. These curves are obtained with 8 MNm outer load and a load angle of 0°. For If a completely stiff tube is attached to a stiff flange surface and is subject to a bending moment, the resulting load distribution has the shape of a sine curve with positive and negative values (see also Figure 1). However, the roller loads in a bearing have the same algebraic sign, as the rollers only transfer pressure loads. For the following figures, the sign of one of the rows was changed to obtain a curve that can be easily compared against the sine shape of a stiff interface.

For the stiff interface, a change in the pitch angle does not affect the individual roller element forces. For a hub/blade interface, this is the case. To illustrate this, the Figure 8 contains changes in $P_{EA}$ (see Equation 3). The $P_{EA}$ of the real interface situation is between 6.2 to 7.4% higher than that of a stiff

interface. This results in lower expected fatigue lifetime. The pitch angle changes this value by 1.2% for 8 MNm and 1.9% for 6 MNm.

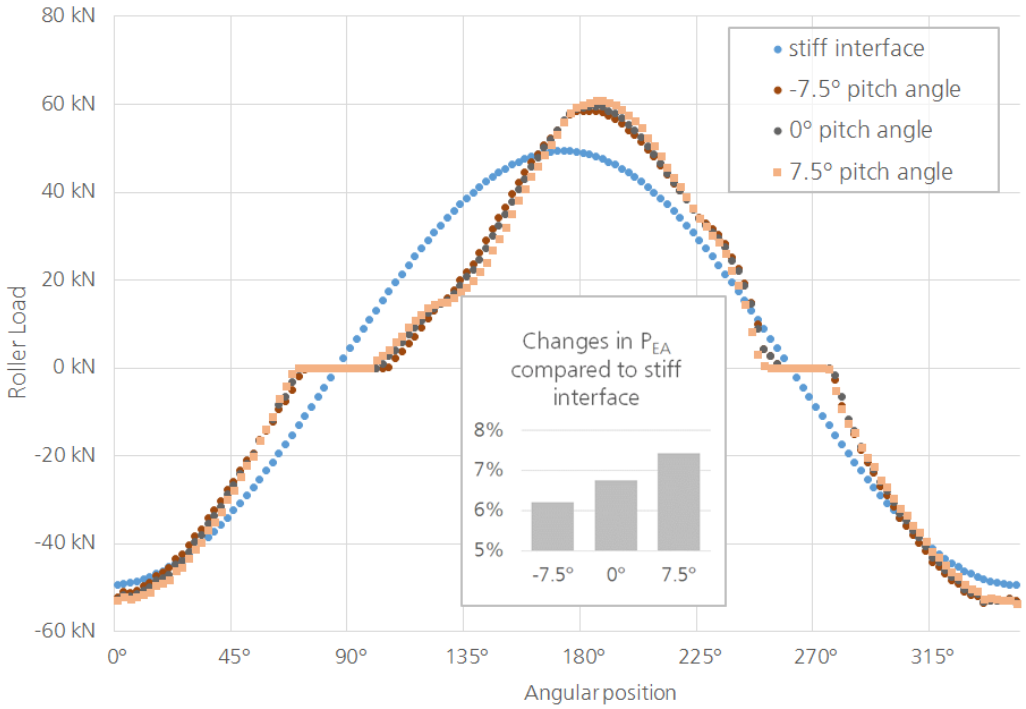


**Figure 8.** Load sharing for 8 MNm outer load, a load angle of 0° and different pitch angles

Figure 9 shows the influence of the load angle for a pitch angle of 0° and an outer load of 8 MNm. A value of -30° generally corresponds to a blade moving upward, while 30° correspond to a downward moving blade. Obviously, the different load angles lead to the loading of different rollers in the bearing. At approximately 90°, a dent in the -30° and +30° curves indicate the location of the pitch drive, which in this model has a significant influence on the roller loads. This influence is less prominent at 30° load angle, however at 30° $P_{EA}$ is 17.3% higher than for the stiff interface. This is also significantly different from the case with 0° load angle. At 6 MNm, the same behavior is observed as well, where the difference between the 0° load angle case and the 30° load angle case is 22.7% of the value obtained with a stiff interface.

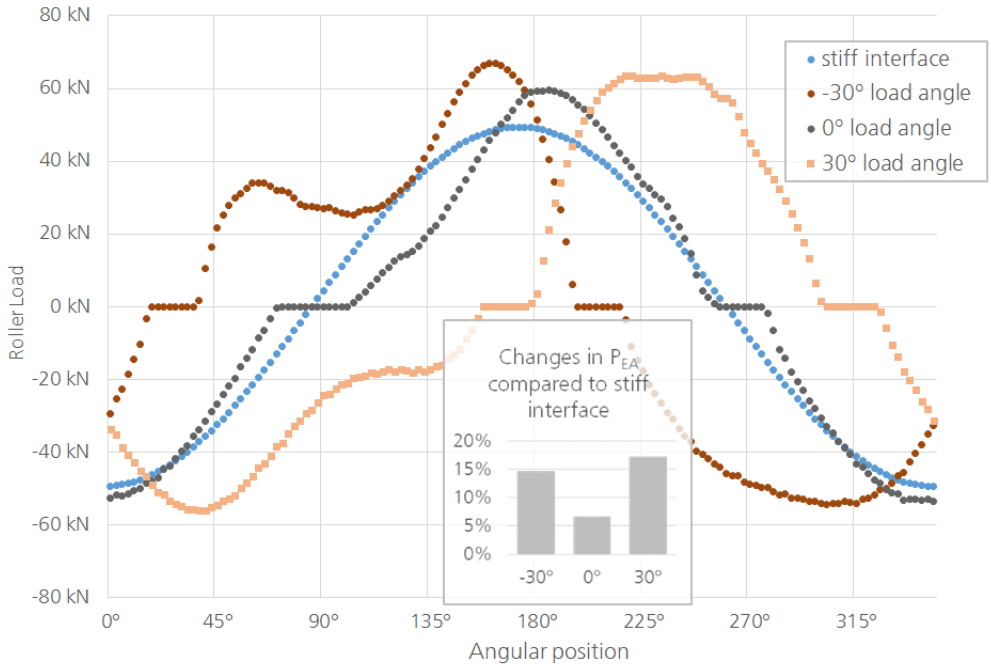


**Figure 9.** Load sharing for 8 MNm outer load, a pitch angle of 0° and different load angles

Table 2 lists $P_{EA}$ for selected parameter combinations and 8 MNm load magnitude. The highest value is 6274.8 kN at -7.5° degree pitch angle and -30° load angle, the lowest value 5743.9 kN at -7.5° pitch angle and 0° load angle. The value for a stiff interface is 5408.5 kN. The range of the values for each load angle varies from 142.6 kN for -30° to 33 kN for 10°, while a clear tendency cannot be recognized.

Table ***3*** presents the results for 6 MNm load magnitude. The highest value is 3850.8 kN at 30° load angle and 7.5° pitch angle, which does not match the parameters for the highest value at 8 MNm.

**Table 2.** Summarized roller loads $P_{EA}$ for selected parameter combinations at 8 MNm load magnitude

| **Load magnitude: 8 MNm** | | | | | | | | |
|---|---|---|---|---|---|---|---|---|
| $P_{EA}$ in kN | | **Load angle** | | | | | | |
| | | **-30°** | **-20°** | **-10°** | **0°** | **10°** | **20°** | **30°** |
| Pitch angle | -7.50° | 6274.8 | 6166.1 | 5930.1 | 5743.9 | 5823.7 | 6108.7 | 6350.0 |
| | -3.75° | 6239.5 | 6154.0 | 5945.0 | 5756.1 | 5811.4 | 6082.6 | 6357.2 |
| | 0.00° | 6203.6 | 6132.5 | 5957.8 | 5773.3 | 5801.0 | 6055.4 | 6343.4 |
| | 3.75° | 6167.2 | 6110.3 | 5959.5 | 5790.6 | 5790.0 | 6029.7 | 6331.4 |
| | 7.50° | 6132.3 | 6069.5 | 5956.4 | 5809.8 | 5792.0 | 6005.1 | 6316.5 |

**Table 3.** Summarized roller loads $P_{EA}$ for selected parameter combinations at 6 MNm load magnitude

| **Load magnitude: 6 MNm** | | | | | | | | |
|---|---|---|---|---|---|---|---|---|
| $P_{EA}$ in kN | | **Load angle** | | | | | | |
| | | **-30°** | **-20°** | **-10°** | **0°** | **10°** | **20°** | **30°** |
| Pitch angle | -7.50° | 3701.3 | 3425.6 | 3122.9 | 2882.6 | 3057.1 | 3467.4 | 3775.8 |
| | -3.75° | 3713.2 | 3406.5 | 3118.8 | 2891.4 | 3043.2 | 3457.6 | 3797.8 |
| | 0.00° | 3683.2 | 3421.8 | 3115.3 | 2897.1 | 3037.7 | 3448.6 | 3819.0 |
| | 3.75° | 3678.9 | 3392.2 | 3108.5 | 2908.6 | 3047.8 | 3439.9 | 3836.8 |
| | 7.50° | 3677.7 | 3392.9 | 3102.3 | 2921.0 | 3025.9 | 3428.5 | 3850.8 |

## 4. Conclusions

In this work, we have presented a comprehensive method to simulate the load distribution in a wind turbine blade bearing. We have used a three-row roller bearing as example and have showed the influence of pitch angle, load angle and load magnitude on the load sharing of the two axial rows of this bearing.

The influence of the pitch angle was evaluated for a pitch angle range of 15° which covers most production states of the turbine. The difference in the resulting summarized roller load $P_{EA}$ is within a range of a few percent, which is a relatively low value. The characteristic of the load sharing is optically similar for all pitch angles. These two findings suggest that it is reasonable to neglect pitch angle influence for fatigue lifetime calculations of pitch bearings.

The load angle has a more dominant influence both on the resulting $P_{EA}$ and the load sharing of the individual rollers. We evaluated this influence for a range of 60° (+/- 30°) of the load angle. All deviations from 0° load angle lead to higher $P_{EA}$. Both this and the different load distribution, which results in different areas of the raceway being subject to fatigue loads, should be taken into account for fatigue and static calculations of blade bearings. The influence of the outer load magnitude on $P_{EA}$ is, as expected, significant. This influence is significant with any bearing application, independent of the specific interface characteristics we evaluated in this work.

We conclude that the structural behavior of the blade causes most of the changes in load sharing and summarized loads. However, the hub should not be neglected as it has been shown in previous publications that a certain influence on the load distribution is caused by this part as well. In the simulations performed for this work, a significant influence of the pitch gear interface on the bearings loads was experienced near the gear interface. While the summarized roller loads where not affected by this and the individual roller loads outside of the gear area show reasonable results, it is still doubtful if the magnitude if this influence can be found in reality as well. Instead of a combination of stiff springs and MPC184 connections, a RBE3 (constraint equation) connection of a section of the bearing ring attached to the blade with a master node which rotational degree of freedom is blocked might provide more realistic results.

Future work in this field will adapt the parameter selection according to the achieved results. The results will also be used as input values for fatigue lifetime calculations of blade bearings.

## 5. Acknowledgements

The present work was carried out with the project “HAPT – Highly Accelerated Pitch Bearing Tests” (Project number 0325918A). The project funding by the German Federal Ministry for Economic Affairs and Energy is kindly acknowledged.

## References

[1] Stammler M and Reuter A 2015 *Blade bearings: damage mechanisms and test strategies (Conference for Wind Power Drives)* (Aachen)
[2] Burton T 2011 *Wind energy handbook* 2nd edn (Chichester, New York: Wiley)
[3] Daidie A, Chaib Z and Ghosn A 2008 3D Simplified Finite Elements Analysis of Load and Contact Angle in a Slewing Ball Bearing *Journal of Mechanical Design* **2008**
[4] Steinkuhl F and Wenske J 2017 *Emulation of interface Stiffnesses for full Scale Tests on Wind Turbine Blade Bearing (DEWEK 2017, 13th Germany Wind Energy Conference)* (Bremen)
[5] Bleich O, Meng F, Daniele E, Thomas P and Popko W 2016 *IWES WIND TURBINE IWT-7.5-164 REV. 2.5* (Fraunhofer IWES)
[6] Aguirrebeitia J, Abasolo M, Avilés R and Fernández de Bustos I 2012 General static load-carrying capacity for the design and selection of four contact point slewing bearings *Finite Elements in Analysis and Design* **55** 23–30
[7] Chen G and Wen J 2012 Load Performance of Large-Scale Rolling Bearings With Supporting Structure in Wind Turbines *J. Tribol.* **2012**
[8] Smolnicki T and Rusiński E 2006 Superelement-Based Modeling of Load Distribution in Large-Size Slewing Bearings *Journal of Mechanical Design* **129**
[9] Gao X H, Huang X D, Wang H and Chen J 2011 Modelling of ball-raceway contacts in a slewing bearing with non-linear springs *Proceedings of the IMechE* **225** 827–31
[10] Schwack F, Prigge F and Poll G 2017 *Frictional Work in Oscillating Bearings – Simulation of an Angular Contact Ball Bearing under Dry Conditions and Small Amplitudes (6th World Tribology Conference)* (Beijing, China)
[11] Schwack F, Stammler M, Flory H and Poll G 2016 Free Contact Angles in Pitch Bearings and their Impact on Contact and Stress Conditions *WindEurope Conference, Hamburg*
[12] Qiu M, Yan J F, Chen L and Zhao B H 2010 Static Analysis on Slewing Bearing with Negative Clearance Based on ANSYS *AMM* **42** 196–9
[13] Harris T A and Kotzalas M N 2007 *Rolling bearing analysis* 5th edn (Boca Raton: CRC, Taylor & Francis)
[14] Stammler M, Schwack F, Bader N, Reuter A and Poll G 2018 Friction torque of wind-turbine pitch bearings – comparison of experimental results with available models *Wind Energ. Sci.* **3** 97–105
[15] DIN ISO 2010 Wälzlager - Dynamische Tragzahlen und nominelle Lebensdauer (ISO 281:2007) *(*DIN ISO 281*)* (Berlin: Beuth)
[16] DIN ISO 2009 Wälzlager - Statische Tragzahlen (ISO 76:2006) *(*DIN ISO 76*)* (Berlin: Beuth)